

Anisotropic ideal strengths and chemical bonding of wurtzite BN in comparison to zincblende BN

R. F. Zhang* and S. Veprek

Department of Chemistry, Technical University Munich, Lichtenberg Strasse 4, D-85747 Munich, Germany

A. S. Argon

Department of Mechanical Engineering, Massachusetts Institute of Technology,
77 Massachusetts Avenue, Cambridge, Massachusetts 02139, USA

(Received 13 March 2008; published 22 May 2008)

The ideal strengths, electronic density of states, and charge density difference of wurtzite w -BN had been calculated by *ab initio* density functional theory and compared to zincblende c -BN. Both polymorphs show a different stacking of lattice planes but have comparable anisotropic strengths, which are due to the similar bonding of three-dimensional sp^3 covalent networks, comparable bond lengths, and charge transfer between the boron and nitrogen atoms.

DOI: 10.1103/PhysRevB.77.172103

PACS number(s): 62.20.-x, 71.20.-b, 71.15.Mb, 73.63.Bd

Among many polymorphs of boron nitrides, two dense BN phases with zincblende (c -BN) and wurtzite (w -BN) structures possess interesting properties such as extreme hardness, high melting point, high thermal conductivity, low dielectric constant, large band gap, etc., which are very useful in many technical applications.^{1,2} The c -BN is stable under high pressure and high temperature, whereas the w -BN coexists with c -BN at a lower temperature. The Vickers hardness of single crystal c -BN is about 48–50 GPa, which is lower than that of diamond (70–100 GPa).^{3,4} The wurtzite boron nitride has been investigated to a lesser extent than c -BN because of its difficulty to prepare a pure phase. It is formed together with c -BN during the high-pressure transformation of h -BN at a somewhat lower temperature of about 1800–2200 K and a pressure of 16–20 GPa.^{5,6} Both c -BN and w -BN have an sp^3 -bonded structure and their Madelung constants are almost identical. Recently, Dubrovinskaia *et al.* reported a synthesis of superhard boron nitride nanocomposites with a load-invariant hardness of 85 GPa.^{5,6} The origin of the hardness enhancement by a factor of about two in the nanocomposites consisting of a mixture of c -BN and w -BN with an average crystallite size of 14 nm has been attributed to the “nanosize effect” and two-phase compositions.⁵ In this Brief Report, we present a comparative study of the ideal tensile and shear strengths, and the bonding nature of both polymorphs by means of *ab initio* density functional theory (DFT) in order to check if the w -BN component phase may contribute to the observed hardness enhancement.

The ideal decohesion and shear strengths of about $(\gamma_S \cdot E_Y / d_0)^{0.5}$ and $G \cdot b / (2\pi \cdot d_0) \approx 0.1 \cdot G$, respectively^{7,8} (where G and E_Y are the shear and Young’s modulus, γ_S is the surface energy, b is the interatomic distance in the shear direction, and d_0 is the interplanar spacing), represent the upper limit of strength that a real material can achieve. It correlates with the onset of dislocation formation and plastic deformation in an ideal crystal.^{9–11} The strength of engineering materials is limited by flaws such as dislocations, microcracks, grain boundaries, and others, and it is usually orders of magnitude smaller than the ideal one.^{12,13} The anisotropic ideal strength, i.e., the maximum stress at which a perfect

crystal becomes mechanically unstable under a given homogenous deformation, can, nowadays, be obtained from *ab initio* calculations.^{14–16} However, care has to be exercised when correlating ideal strength with hardness because the latter depends in a complex manner on many factors such as flaws in real materials and the type of loading during the hardness measurement.^{7,8}

The present *ab initio* DFT calculations were done by means of the VASP code¹⁷ with the projector augmented wave method employed to describe the electron-ion interaction and the generalized-gradient approximation for the exchange-correlation term. The integration in the Brillouin zone has been done on special k points of $9 \times 9 \times 9$ grids for the phases that were under consideration, which were determined according to the Monkhorst–Pack scheme, the energy cutoff of 600 eV, and the tetrahedron method with Blöchl corrections for the energy and smearing methods for the stress calculations. The verification of the reliability of our calculations has been done by calculating the total energies, equilibrium lattice parameter, and bulk modulus of c -BN, and comparing them to the published data,¹⁸ as described in our earlier papers that are also for other systems.¹⁹

Here, we describe the calculations of the stress-strain relationships.^{14–16,19} First, the atomic basis vectors of a given crystal cell were projected onto the Cartesian coordinates (R) with one axis vector being parallel to the imposed strain direction for the tension. For the shear, one axis vector was perpendicular to the slip plane and another one was parallel to the slip direction in the plane. Afterwards, the crystal has been incrementally deformed by transforming the unstrained atomic basis vector matrices R to the strained ones R' using the deformation matrices

$$R' = R \cdot \begin{pmatrix} 1 + e_1 & \frac{1}{2}e_6 & \frac{1}{2}e_5 \\ \frac{1}{2}e_6 & 1 + e_2 & \frac{1}{2}e_4 \\ \frac{1}{2}e_5 & \frac{1}{2}e_4 & 1 + e_3 \end{pmatrix},$$

where $e_1 = e_{xx}$, $e_2 = e_{yy}$, $e_3 = e_{zz}$, $e_4 = e_{zy} + e_{yz}$, $e_5 = e_{zx} + e_{xz}$, and $e_6 = e_{yx} + e_{xy}$ are the strain components in the Voigt notation.

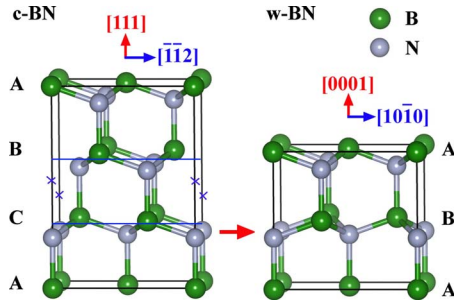


FIG. 1. (Color online) Crystallographic stacking sequence in a redefined orthorhombic cell for (a) *c*-BN with $[1\bar{1}\bar{0}]$, $[\bar{1}\bar{1}\bar{2}]$, and $[111]$, and (b) for *w*-BN with $[\bar{1}\bar{2}\bar{1}\bar{0}]$, $[10\bar{1}\bar{0}]$, and $[0001]$, as the cell axes vectors, respectively.

The diagonal strain components e_{xx} , e_{yy} , and e_{zz} represent the tension while the off-diagonal components represent the shear. In order to keep the crystal under a stress state of uniaxial tension or shear, the strained cell has been relaxed for both the atomic basis vectors and for the atom coordinates inside the unit cell by keeping the applied strain component fixed and relaxing the other five strain components until their conjugate stress components (i.e., Hellmann–Feynman stresses) reached negligible values. To ensure that the strain path is continuous, the starting position at each strain step has been taken from the relaxed coordinates of the previous strain step. In the instance of having a large strain, the crystal symmetry may be changed and the Brillouin zone significantly deformed and so, we verified the convergence of the calculations of the stress-strain curves by using two different meshes with $9 \times 9 \times 9$ and $11 \times 11 \times 11$ k points. The calculated stress-strain curves in the tension along the $\langle 111 \rangle$ direction were identical within less than 1%, and the ideal strength of 55.258 GPa has been obtained for both meshes. Furthermore, we repeated the calculation for the $\langle 111 \rangle$ tension using a higher cutoff energy of 800 eV and obtained a value of 55.04 GPa, which is only about 0.4% lower than the above mentioned one. Our calculated stress-strain curves for TiN and Si_3N_4 were also in reasonable agreement with the previous calculations.¹⁹

The structural relationship between *c*-BN and *w*-BN is given by different stacking sequences ABCA... along the $[111]$ direction and ABA... along the $[0001]$ direction, respectively (Fig. 1). Thus, the $\langle 111 \rangle$, $\langle 1\bar{1}\bar{0} \rangle$, and $\langle \bar{1}\bar{1}\bar{2} \rangle$ directions of *c*-BN are chosen to compare to $\langle 0001 \rangle$, $\langle \bar{1}\bar{2}\bar{1}\bar{0} \rangle$, and $\langle 10\bar{1}\bar{0} \rangle$ directions of *w*-BN. Note that the direction indicated in a bracket $\langle hkl \rangle$ means that, if for a given $[hkl]$ direction, the lattice symmetry exists with respect to the opposite direction $[\bar{h}\bar{k}\bar{l}]$, the calculated stress-strain curve also applies for the opposite direction.

Figure 2 shows the stress-strain relationships for *c*-BN in comparison to those for *w*-BN. The ideal tensile strengths [Fig. 2(a)] for *w*-BN in the $\langle \bar{1}\bar{2}\bar{1}\bar{0} \rangle$ direction and for *c*-BN in the $\langle 1\bar{1}\bar{0} \rangle$ direction are about 90.6 and 84.1 GPa, respectively, which is much larger than for the two other orthogonal directions. The anisotropy ratio of ideal tensile strengths

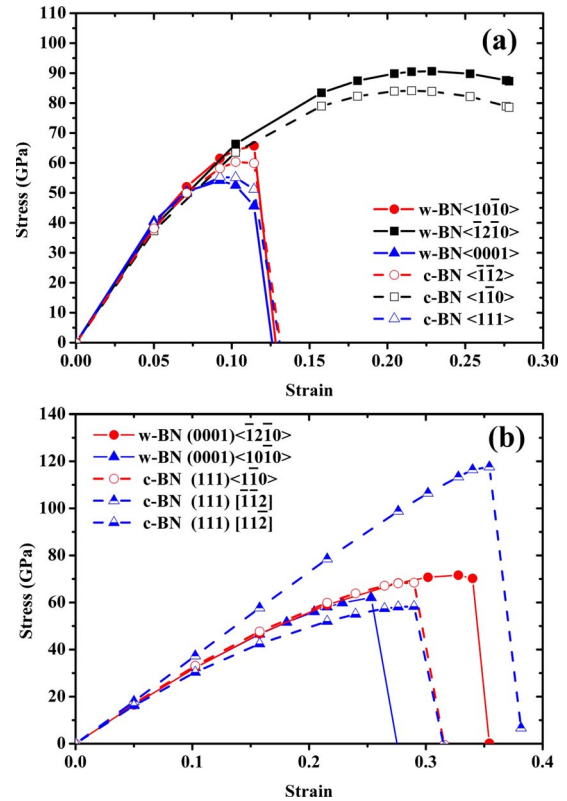


FIG. 2. (Color online) Stress-strain relationships calculated by *ab initio* DFT method for both dense BN polymorphs: (a) tension and (b) shear. Note that with consideration of the crystallographic similarity (see Fig. 1), the lattice directions of $\langle 0001 \rangle$, $\langle \bar{1}\bar{2}\bar{1}\bar{0} \rangle$, and $\langle 10\bar{1}\bar{0} \rangle$ for *w*-BN were chosen to be compared to $\langle 111 \rangle$, $\langle 1\bar{1}\bar{0} \rangle$, and $\langle \bar{1}\bar{1}\bar{2} \rangle$ for *c*-BN, respectively.

for *w*-BN is $\sigma_{\langle \bar{1}\bar{2}\bar{1}\bar{0} \rangle} = 90.6$ GPa: $\sigma_{\langle 10\bar{1}\bar{0} \rangle} = 65.7$ GPa: $\sigma_{\langle 0001 \rangle} = 54.1$ GPa $\approx 1.67:1.21:1$, which is similar to that of *c*-BN of $\sigma_{\langle 1\bar{1}\bar{0} \rangle} = 84.1$ GPa: $\sigma_{\langle \bar{1}\bar{1}\bar{2} \rangle} = 60.3$ GPa: $\sigma_{\langle 111 \rangle} = 55.3$ GPa $\approx 1.53:1.09:1$. The weakest direction in *w*-BN is $\langle 0001 \rangle$ with an ideal tensile strength of 54.1 GPa, which compares to the lowest tensile strength of 55.3 GPa for *c*-BN along the $\langle 111 \rangle$ directions.

The plastic deformation occurs in the shear. Therefore, in order to understand the strength of both polymorphs, one has to determine the ideal shear strengths in the relevant slip systems, as well as the bonding nature.^{18,19} The lowest shear strength of 62.1 GPa for *w*-BN is found in the $(0001) \langle 10\bar{1}\bar{0} \rangle$ slip systems [Fig. 2(b)]. This value is slightly higher than the 58.3 GPa found for the $(111) [1\bar{1}\bar{2}]$ slip system of *c*-BN. However, in accord with the previous studies,^{14,18} the shear deformations of *c*-BN along the $(111) [\bar{1}\bar{1}\bar{2}]$ slip system are asymmetric with respect to the opposite shear direction $(111) [1\bar{1}\bar{2}]$, as seen in Fig. 2(b). This is due to the three-layers stacking (ABCA...) in the $\langle 111 \rangle$ direction, which is asymmetric for the shear deformation. The shear modulus is important in the modeling of crystal plasticity.^{12,13} From Fig. 2(b), we estimate its average value from the slope of the stress-strain curves for a small strain of about 327 ± 3 GPa for both polymorphs.

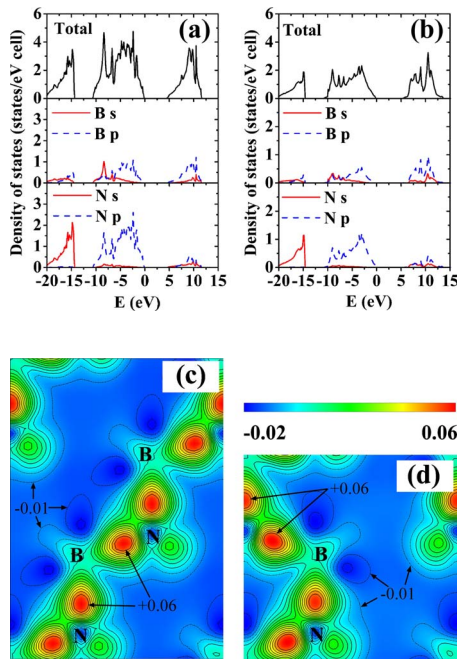


FIG. 3. (Color online) Total and partial electronic density of states for (a) *c*-BN and (b) *w*-BN, and valence charge density difference with respect to the orthorhombic cells of (c) *c*-BN in the $(1\bar{1}0)$ plane and (d) *w*-BN in the $(\bar{1}2\bar{1}0)$ plane, respectively. The color scale of the valence charge density difference in (c) and (d) is in units of [electrons/bohr³].

A further understanding of the properties of both polymorphs yields the electronic density of states (DOS) and charge density difference (CDD), which were calculated and are shown in Fig. 3. The total DOS for both dense BN polymorphs presents three regions: The lower part of the valence bands is dominated by N $2s$ states, and the upper part by N $2p$ -, and B $2s$ - and $2p$ -like states. Both the *c*-BN [Fig. 3(a)] and the *w*-BN [Fig. 3(b)] are wide band gap semiconductors with calculated band gaps of about 4.6 and 5.2 eV, respectively, which can reasonably compare to the theoretical values of 5.18 and 5.81 reported in Ref. 20. There are no experimental data of the value of the band gap for *w*-BN because of the difficulties in preparing high quality samples. Our value for *c*-BN is smaller than the experimental one of about 6 eV reported in Ref. 1 but this applies to all the theoretical results calculated by the *ab initio* methods (e.g., the already mentioned value of 5.18 eV reported in Ref. 20 and the even lower value of 4.5 eV calculated by MacNaugh-

ton *et al.*²¹). The valence bandwidth of *c*-BN of about 11 eV, which is dominated by the overlapping of N $2p$ -, and B $2s$ - and $2p$ -orbitals, is close to that of *w*-BN whose width is about 10.5 eV.

The bond strength and charge transfer can be further characterized by CDD, as shown in Figs. 3(c) and 3(d), for the *c*-BN and the *w*-BN, respectively. The CDD is defined as the difference between the calculated total charge density of the crystal and the superposition of the charge densities of neutral atoms. A positive value (red color and solid contours) means an increase in the negative charge while a negative value (blue color and dotted contours) means its decrease, as compared to the neutral atoms. The strong directional bonds between B-N pairs can be seen as the significant charge accumulation [red color regions in Figs. 3(c) and 3(d)] between the B-N bond pairs. One can clearly see that the difference of the valence charge density distribution is almost indistinguishable for both polymorphs; thus, confirming that the B-N bond strengths are similar. This is further supported by the fact that the B-N bond length of 0.15693 and 0.15827 nm that were calculated for *c*-BN and *w*-BN, respectively, differ only by 0.8%.

Because the difference of ideal strengths and shear moduli are small for both dense BN polymorphs and their chemical bonding is similar, the difference of the intrinsic mechanical and electronic properties of both polymorphs cannot explain the significant hardening for the *w*-BN/*c*-BN nanocomposites reported by Dubrovinskaia *et al.*⁵ The hardness enhancement of the *c*-BN/*w*-BN nanocomposites by a factor of two can be easily explained in terms of a decreasing dislocation activity with a decreasing crystallite size before the “inverse Hall–Petch” due to grain boundary sliding becomes significant (for reviews, see Refs. 4 and 22). This is in agreement with the earlier phenomenological (Ref. 23), numerical (Ref. 24), and recent analytical models of the “strongest size” (Ref. 25). The possible contribution of the quantum confinement, as suggested in Ref. 5, requires further study.

In conclusion, we studied the structural, mechanical, and electronic properties of two dense BN polymorphs by means of *ab initio* DFT calculations. The comparable ideal strengths, shear modulus, and the similar nature of covalent bonds show that both polymorphs are intrinsically strong solids.

This work was supported by the German Research Foundation (DFG). We also gratefully acknowledge the Leibniz computer center.

*Author to whom correspondence should be addressed. FAX: +49-90-28913626; ruifeng.zhang@lrz.tum.de

¹P. B. Mirkarimi, K. F. McCarty, and D. L. Medlin, *Mater. Sci. Eng., R.* **21**, 47 (1997).

²A. Mujica, A. Rubio, A. Munoz, and R. J. Needs, *Rev. Mod. Phys.* **75**, 863 (2003).

³D. He, Y. Zhao, L. Daemen, J. Qian, T. D. Shen, and T. W.

Zerda, *Appl. Phys. Lett.* **81**, 643 (2002).

⁴S. Veprek, *J. Vac. Sci. Technol. A* **17**, 2401 (1999), and references therein.

⁵N. Dubrovinskaia, V. L. Solozhenko, N. Miyajima, V. Dmitriev, O. O. Kurakevych, and L. Dubrovinsky, *Appl. Phys. Lett.* **90**, 101912 (2007).

⁶D. Rafaja, V. Klemm, M. Motylenko, M. R. Schwarz, T. Bar-

- sukova, E. Kroke, D. Frost, L. Dubrovinsky, and N. Dubrovinskaia, *J. Mater. Res.* **23**, 981 (2008).
- ⁷F. A. McClintock and A. S. Argon, *Mechanical Behavior of Materials* (Addison-Wesley, Reading, MA, 1966), pp. 118 and 489.
- ⁸A. Kelly and N. H. Macmillan, *Strong Solids*, 3rd ed. (Clarendon, Oxford, 1986), pp. 1–56.
- ⁹A. Gouldstone, K. J. Van Vliet, and S. Suresh, *Nature (London)* **411**, 656 (2001).
- ¹⁰J. Li, K. J. Van Vliet, T. Zhu, S. Yip, and S. Suresh, *Nature (London)* **418**, 307 (2002).
- ¹¹K. J. Van Vliet, J. Li, T. Zhu, S. Yip, and S. Suresh, *Phys. Rev. B* **67**, 104105 (2003).
- ¹²J. Haines, J. M. Leger, and G. Bocquillon, *Annu. Rev. Mater. Res.* **31**, 1 (2001).
- ¹³V. V. Brazhkin, A. G. Lyapin, and R. J. Hemley, *Philos. Mag. A* **82**, 231 (2002).
- ¹⁴Y. Zhang, H. Sun, and C. F. Chen, *Phys. Rev. Lett.* **93**, 195504 (2004); **94**, 145505 (2005).
- ¹⁵D. Roundy, C. R. Krenn, M. L. Cohen, and J. W. Morris, Jr., *Phys. Rev. Lett.* **82**, 2713 (1999); *Philos. Mag. A* **81**, 1725 (2001).
- ¹⁶S. Ogata, J. Li, N. Hirotsuki, Y. Shibutani, and S. Yip, *Phys. Rev. B* **70**, 104104 (2004); S. Ogata, J. Li, and S. Yip, *Science* **298**, 807 (2002).
- ¹⁷G. Kresse and J. Hafner, *Phys. Rev. B* **47**, 558 (1993); **49**, 14251 (1994).
- ¹⁸R. F. Zhang, S. Veprek, and A. S. Argon, *Appl. Phys. Lett.* **91**, 201914 (2007).
- ¹⁹R. F. Zhang, S. H. Sheng, and S. Veprek, *Appl. Phys. Lett.* **90**, 191903 (2007); R. F. Zhang, S. H. Sheng, and S. Veprek, *ibid.* **91**, 031906 (2007); R. F. Zhang, S. H. Sheng, and S. Veprek, *Phys. Rev. B* **76**, 075208 (2007).
- ²⁰Y. N. Xu and W. Y. Ching, *Phys. Rev. B* **44**, 7787 (1991).
- ²¹J. B. MacNaughton, A. Moewes, R. G. Wilks, X. T. Zhou, T. K. Sham, T. Taniguchi, C. Y. Chan, W. J. Zhang, I. Bello, S. T. Lee, H. Hofmann, and K. Watanabe, *Phys. Rev. B* **72**, 195113 (2005).
- ²²R. W. Siegel and G. E. Fougere, *Nanostruct. Mater.* **6**, 205 (1995).
- ²³J. E. Carsley, J. Ning, W. W. Milligan, S. A. Hackney, and E. C. Aifantis, *Nanostruct. Mater.* **5**, 441 (1995).
- ²⁴J. Schiotz, F. D. Di Tolla, and K. W. Jacobsen, *Nature (London)* **391**, 561 (1998).
- ²⁵A. S. Argon and S. Yip, *Philos. Mag. Lett.* **86**, 713 (2006); S. Yip, *Nature (London)* **391**, 532 (1998).